CHEMISTRY
AN ASIAN JOURNAL

DOI: 10.1002/asia.200600350

Synthesis of Molecular Wires of Linear and Branched Bis(terpyridine)-Complex Oligomers and Electrochemical Observation of Through-Bond Redox Conduction

Yoshihiko Nishimori, Katsuhiko Kanaizuka, Masaki Murata, and Hiroshi Nishihara*[a]

Abstract: Films of linear and branched oligomer wires of $Fe(tpy)_2$ (tpy = 2,2′:6′,2″-terpyridine) were constructed on a gold-electrode surface by the interfacial stepwise coordination method, in which a surface-anchoring ligand, $(tpy{-}C_6H_4N{=}NC_6H_4{-}S)_2$ (**1**), two bridging ligands, $1,4\text{-}(tpy)_2C_6H_4$ (**3**) and $1,3,5\text{-}(C{\equiv}C{-}tpy)_3C_6H_3$ (**4**), and metal ions were used. The quantitative complexation of the ligands and Fe^{II} ions was monitored by electrochemical measurements in up to eight complexation cycles for linear oligomers of **3** and in up to four cycles for branched oligomers of **4**. STM observation of branched oligomers at low surface coverage showed an even distribution of nanodots of uniform size and shape, which suggests the quantitative formation of dendritic structures. The electron-transport mechanism and kinetics for the redox reaction of the films of linear and branched oligomer wires were analyzed by potential-step chronoamperometry (PSCA). The unique current-versus-time behavior observed under all conditions indicates that electron conduction occurs not by diffusional motion but by successive electron hopping between neighboring redox sites within a molecular wire. Redox conduction in a single molecular wire in a redox-polymer film has not been reported previously. The analysis provided the rate constant for electron transfer between the electrode and the nearest redox-complex moiety, k_1 (s^{-1}), as well as that for intrawire electron transfer between neighboring redox-complex moieties, k_2 ($cm^2\,mol^{-1}\,s^{-1}$). The strong effect of the electrolyte concentration on both k_1 and k_2 indicates that the counterion motion limits the electron-hopping rate at lower electrolyte concentrations. Analysis of the dependence of k_1 and k_2 on the potential gave intrinsic kinetic parameters without overpotential effects: $k_1{}^0 = 110\ s^{-1}$, $k_2{}^0 = 2.6\times10^{12}\ cm^2\,mol^{-1}\,s^{-1}$ for [*n*Fe**3**], and $k_1{}^0 = 100\ s^{-1}$, $k_2{}^0 = 4.1\times10^{11}\ cm^2\,mol^{-1}\,s^{-1}$ for [*n*Fe**4**] (*n* = number of complexation cycles).

Keywords: bridging ligands · electron transport · molecular wires · oligomers · terpyridine complexes

Introduction

How an electron moves in a single molecular wire is an important and elementary question in molecular science, especially in relation to biological electron-transfer systems[1] and molecular devices.[2] Much recent interest has focused on the electron-transfer characteristics of molecular wires, such as alkyl chains,[3] π-conjugated conducting polymers,[4] DNA,[5] and polypeptides.[6] Redox polymers, in which redox species are connected to form a polymer wire, are representative electron-conducting substances;[7] however, there have been no significant studies on electron transfer within a single redox-polymer wire.

Redox-polymer films on an electrode surface have been prepared mostly by polymer coating, chemical modification, and electrochemical polymerization. Many experimental and theoretical studies on electron-transport behavior have been conducted on such redox-polymer films.[8] Polymer chains have been distributed randomly in these films, in which electron transport has generally been treated according to the concept of "redox conduction" based on the diffusional motion of collective electron-transfer pathways.[9] The apparent diffusion coefficient, D_{app}, for electron conduction in such redox films is composed of electron-hopping and/or physical diffusion terms and is the key factor in terms of the Dahms–Ruff equation[10] and Laviron–Andrieux–Savéant theory.[11] The migration effect and counterion motion are also important with respect to D_{app}.[12] Potential-step chro-

[a] Y. Nishimori, Dr. K. Kanaizuka, Dr. M. Murata, Prof. H. Nishihara
Department of Chemistry
School of Science, The University of Tokyo
Hongo, Bunkyo-ku, Tokyo 113-0033 (Japan)
Fax: (+81) 3-5841-8063
E-mail: nisihara@chem.s.u-tokyo.ac.jp

Supporting information for this article is available on the WWW under http://www.chemasianj.org or from the author.

noamperometry (PSCA) is a simple method for evaluating D_{app}.[13]

Recently, redox-oligomer wires were fabricated on an electrode surface by the interfacial stepwise coordination method.[14] An important advantage of this method is that it affords organized structures of rigid redox-polymer wires with the desired numbers of redox-complex units perpendicular to the surface. It is also possible to prepare desired sequences of different metal-complex units by changing the sources of the metal ion and bridging ligand in the stepwise coordination process. Previously,[15] we reported an accumulation of 47 cobalt-complex units as well as an accumulation of 10 iron- and five cobalt-complex units on a gold surface by using a combination of the surface-anchoring terpyridine ligand (tpy–C_6H_4N=NC_6H_4–S)$_2$ (**1**; tpy = 2,2′:6′,2″-terpyridine), Fe and/or Co ions, and a bridging ligand, tpy–C_6H_4N=NC_6H_4–tpy (**2**).[16] Herein, we describe the use of the two-way-bridging ligand 1,4-(tpy)$_2C_6H_4$ (**3**) and three-way-bridging ligand 1,3,5-(tpy)$_3C_6H_3$ (**4**) to prepare linear and branched oligomer wires, respectively, on a gold surface in the presence of **1** and Fe^{2+} ions. This is a rare example of an attempt to prepare dendritic oligomers on a surface by the stepwise coordination method.[17] The electron-transport behavior in films of such highly organized oligomer wires would be expected to differ from that of previous polymer

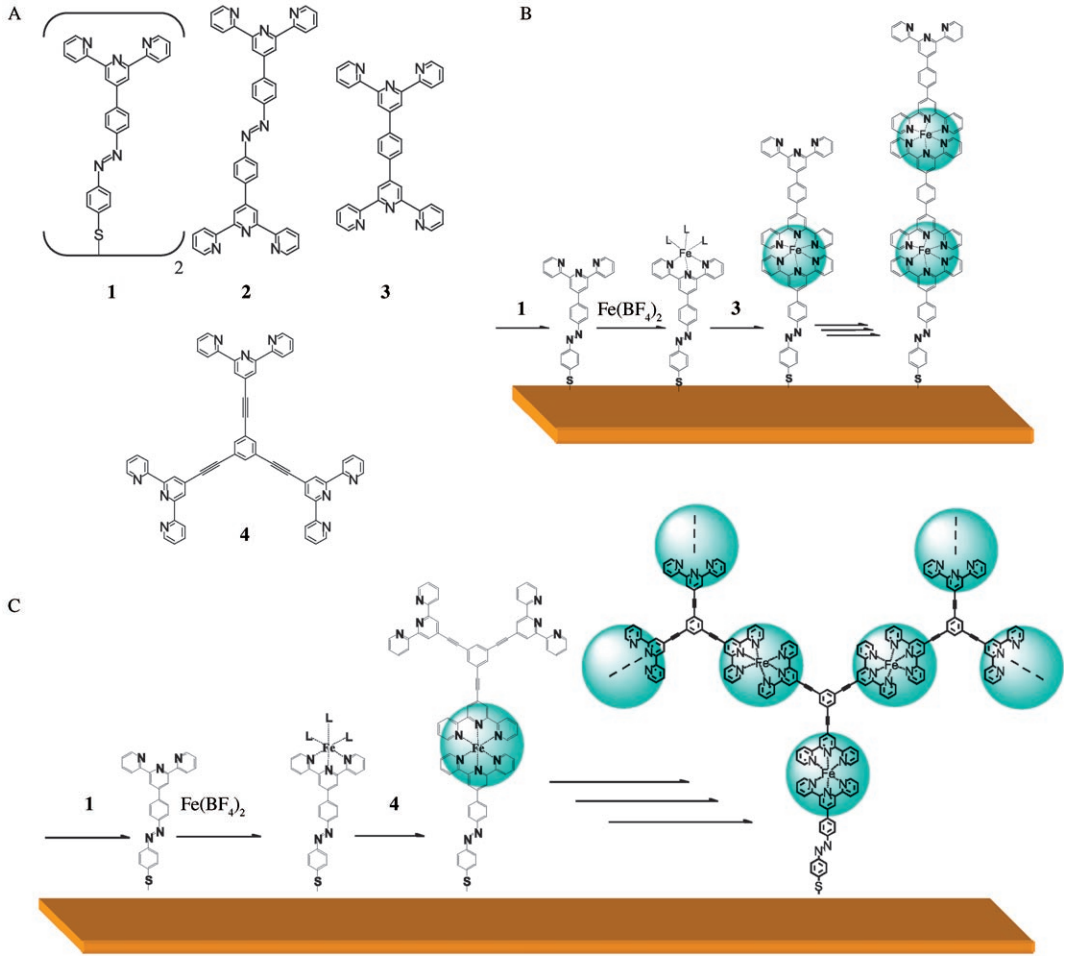

Figure 1. Chemical structures of the ligands used in this study (A), and stepwise coordination methods for the preparation of linear (B) and branched (C) oligomer wires.

Abstract in Japanese:

金表面上で電極固定用配位子(tpy-C_6H_4N=N-C_6H_4-S)$_2$ (tpy = 2,2':6',2''-terpyridine) (**1**)と二種の架橋配位子 1,4-C_6H_4(tpy)$_2$ (**3**)、1,3,5-C_6H_3-(C≡C-tpy)$_3$ (**4**)、および鉄イオンを用いた界面逐次錯形成反応を利用し、一次元鎖状および樹状に Fe(tpy)$_2$ オリゴマーワイヤを作製した。定量的な分子ワイヤの増長を電気化学および STM 測定によって観測した。膜中での電子移動メカニズムをポテンシャルステップクロノアンペロメトリー法で解析したところ、膜中での電子移動は拡散過程で起こるのではなく、分子鎖内で隣接するレドックスサイト間の連続的な電子ホッピングにより起こることが示された。これはレドックス薄膜中での単一分子鎖内電子移動を観測した初めての例である。

CHEMISTRY
AN ASIAN JOURNAL

films containing randomly distributed redox sites. To clarify the "redox conduction" mechanism in the redox-complex oligomer films, we used PSCA to measure the electron-transport kinetics of the Fe^{III}/Fe^{II} couple. We found that the redox conduction in the oligomer films occurs not in a random-walk process (diffusion) but by through-bond electron transport. We describe herein the synthesis and kinetics of the oligomer films, and the analysis of the electron-transport mechanism.

Results and Discussion

Stepwise Construction and Characterization of Iron-Complex Oligomer Wires on Gold

We fabricated linear oligomer wires on gold by a combination of self-assembled monolayer (SAM) formation with a terpyridine derivative and stepwise metal–terpyridine coordination reactions by using the phenylene-bridged bis(terpyridine) ligand **3** in a manner similar to that described in our previous communication, in which the azobenzene-bridged bis(terpyridyl) ligand **2** was used as a bridging ligand (Figure 1).[15,18] In the present case, to accumulate Fe-$(tpy)_2$ units, we used an immersion time in a solution of **1** of $t_1 = 5$ min for SAM preparation, and immersion times of $t_{Fe} = 3$ h in aqueous $Fe(BF_4)_2$ and $t_3 = 3$ h in **3**. Figure 2 shows

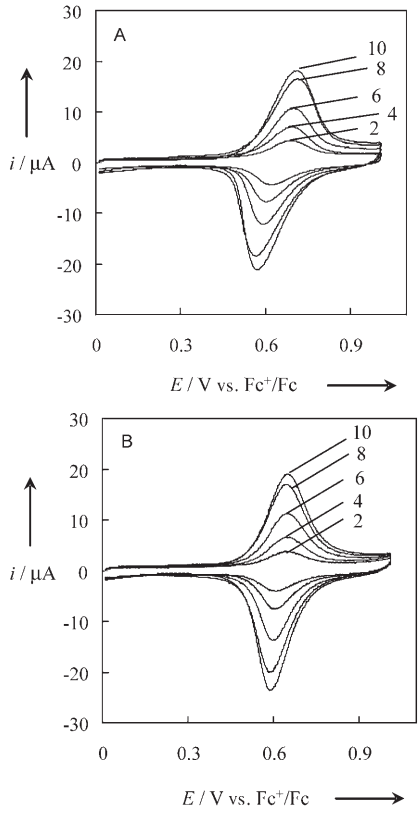

Figure 2. Cyclic voltammograms of [*n*Fe**3**] ($n = 2$, 4, 6, 8, and 10) at a scan rate of 0.1 $V s^{-1}$ in Bu_4NClO_4/CH_2Cl_2 (0.1 mol dm^{-3} (A) and 1 mol dm^{-3} (B)). The numbers assigned to the curves refer to *n*.

the cyclic voltammograms of the Fe^{III}/Fe^{II} couple with changes in the number of metal-complexation cycles, *n*: [2Fe**3**], [4Fe**3**], [6Fe**3**], [8Fe**3**], and [10Fe**3**], in Bu_4NClO_4/CH_2Cl_2 (0.1 and 1 mol dm^{-3}, respectively; see the Supporting Information for cyclic voltammograms in solutions of other electrolyte concentrations). The peak current, i_p, and thus the coverage of redox active sites, Γ (mol cm^{-2}), increased in proportion to *n*, with $\Gamma_{CV,[n\mathrm{Fe}\mathbf{3}]} = 1.0n \times 10^{-10}$ mol cm^{-2} (Figure 3). This Γ value is a little smaller than that for

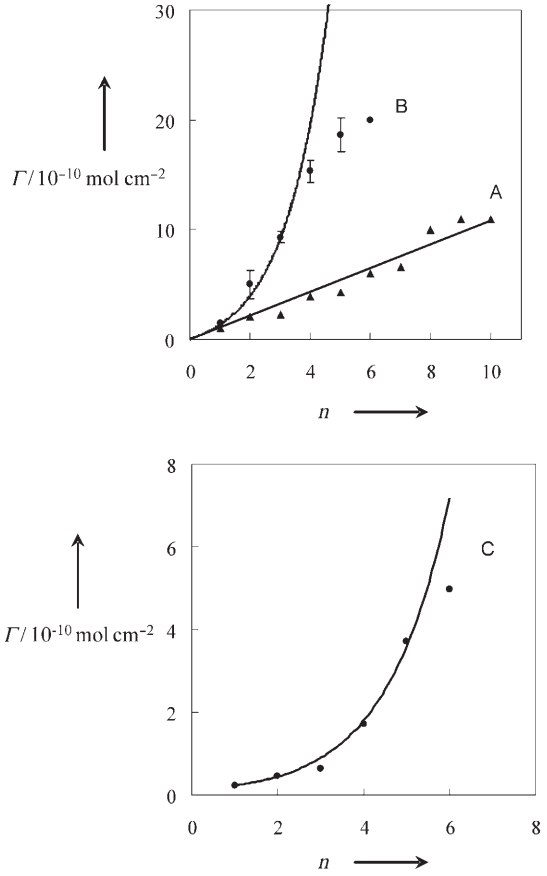

Figure 3. Plots of the coverage of redox-active sites, Γ, versus the number of complexation cycles, *n*, for A) [*n*Fe**3**] ($t_1 = 5$ min), B) [*n*Fe**4**] ($t_1 = 5$ min), and C) [1Fe**3**–(*n*−1)Fe**4**] ($t_1 = 10$ s). The lines denote the relationships $\Gamma = C \times n$ for A, $\Gamma = C(2^n - 1)$ for B, and $\Gamma = C2^{n-1}$ ($n \geq 1$) for C.

[*n*Fe**2**] ($1.2n \times 10^{-10}$ mol cm^{-2}).[15] The peak-to-peak potential separation, ΔE_p, increased slightly with the number of layers in the electrolyte solution of concentration 1 mol dm^{-3}, whereas ΔE_p increased significantly with *n* in the electrolyte solution at 0.1 mol dm^{-3} (compare Figures 2A and B). This change in ΔE_p suggests, as a primary interpretation, that the "resistance of the film" (see discussion below) is higher when the electrolyte concentration is lower. The voltammogram did not change significantly at electrolyte concentrations above 1 mol dm^{-3}, which can be explained by the fact that the concentration of redox sites in the film is estimated to be 1 mol dm^{-3}. This value is much higher than the regular concentration of redox species in solution, which can be as

high as several mmol dm^{-3} for voltammetry of this type. An electrolyte concentration of 0.1 mol dm^{-3} was usually used in the previous electrochemical studies on redox-polymer films, whereas the concentrations of redox-active species in the film were as high as that in the present study.[8,9,19]

The new three-way-bridging ligand **4** was prepared by the Stille coupling of tpy–C≡CS*n*Bu$_3$ with 1,3,5-C$_6$H$_3$Br$_3$ in the presence of [Pd(PPh$_3$)$_4$] as the catalyst. We developed a branched molecular wire of Fe(tpy)$_2$ units by the stepwise coordination method with **1** and **4**. In this case, Γ can be expected to increase with the number of complexation cycles, n, that have a 2^n-1 relationship if no interwire or wire-to-gold surface steric repulsion perturbs the coordination reaction at the terminals of the molecular wires. (The film for the nth complexation cycle is abbreviated as [nFe**4**]). Figure 4 shows cyclic voltammograms of [2Fe**4**], [3Fe**4**], and

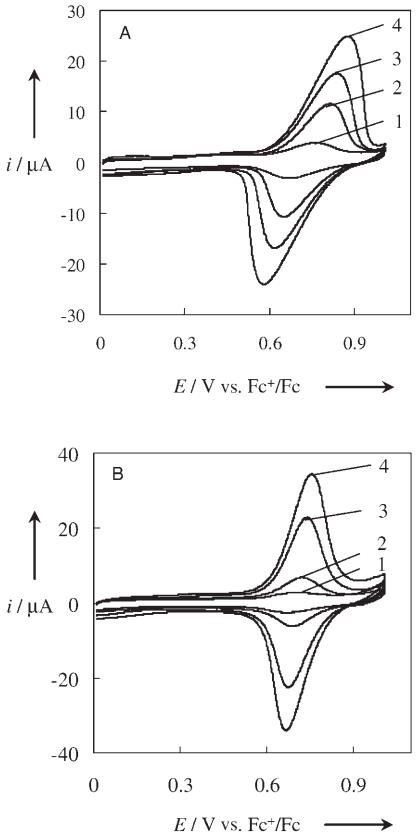

Figure 4. Cyclic voltammograms of [nFe**4**] (n=1, 2, 3, and 4) at a scan rate of 0.1 V s^{-1} in Bu$_4$NClO$_4$/CH$_2$Cl$_2$ (0.1 mol dm^{-3} (A) and 1 mol dm^{-3} (B)). The numbers assigned to the curves refer to n.

[4Fe**4**] prepared by using immersion times of t_1=5 min, t_{Fe}=3 h, and t_4=3 h in Bu$_4$NClO$_4$/CH$_2$Cl$_2$ (0.1 and 1 mol dm^{-3}, respectively; cyclic voltammograms in solutions of other electrolyte concentrations are shown in the Supporting Information). The $\Gamma_{CV,[n\text{Fe}4]}$ values estimated from the amount of electricity in the anodic peak of the cyclic voltammogram are shown in Figure 3, whereby an increase in Γ according to the relationship 2^n-1 occurred up to about n=4. Calculation of the molecular structure by using MM+ indicates that the higher-generation redox sites can penetrate through gaps in the lower-generation sites (see the Supporting Information). Consequently, the volume concentration of the redox sites was expected to increase with increasing n. When n was higher than 4, the rate of increase in Γ decreased until it was similar to those for linear polymers, such as [nFe**3**]. This observation indicates that steric repulsion between complex sites becomes crucial at higher values of n; as a result, the wire can extend in only one dimension. Recently, Rubinstein and co-workers reported similar formation of a branched molecular wire through a coordination reaction with Zr^{4+} ions. In that case, ellipsometry and contact-angle measurements indicated steric-hindrance effects in higher generations.[17]

STM images of the films with branched polymer wires, [2Fe**4**] (t_1=5 min) and [1Fe**3**–3Fe**4**] (t_1=10 s), are shown in Figure 5. The STM image of the linear-oligomer film [2Fe**2**] (t_1=5 min) displays near close-packing with circular domains of 6-nm o.d. (outside diameter), which indicates a stacking of molecular chains as reported previously.[15] The image of the film [2Fe**4**] of branched oligomer wires shows clearer domain structures with an even distribution of shape and size over the whole surface (Figure 5A). In contrast, the

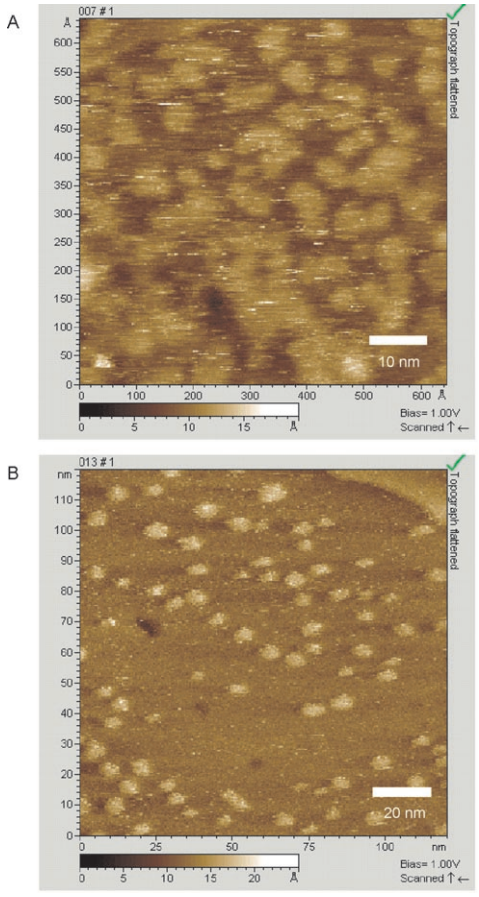

Figure 5. STM images of the films with branched wires. A) [2Fe**4**] (t_1=5 min); B) [1Fe**3**–3Fe**4**] (t_1=10 s).

CHEMISTRY
AN ASIAN JOURNAL

STM image of [1 Fe**3**–3 Fe**4**] ($t_1 = 10$ s), which was constructed through one complexation cycle with the two-way-bridging ligand **3** followed by two complexation cycles with the three-way-bridging ligand **4**, displays sparse distribution of the branched oligomer wires as bright and uniform circular dots with a diameter of 6 nm, similar to the size of the expected structure (Figure 5B). The STM images of branched oligomer wires of different generations [1 Fe**3**–*n* Fe**4**] ($n = 2$–5) show circular dots, the diameters of which increase with the number of complexation cycles (see the Supporting Information). These results strongly suggest the formation of ideal structures on the surface by the stepwise coordination method, whereas the STM images do not directly reflect the morphology of the surface.[19]

Electron Transport in Films of Fe(tpy)$_2$-Oligomer Wires on Gold

If the redox conduction occurs through diffusional motion, and if the diffusion process within the film is the rate-determining step (i.e., if the kinetics of electron transfer between the electrode and the nearest redox sites in the film are sufficiently fast), the current–time curve after the potential step that causes the redox reaction of the redox-polymer film obeys the Cottrell equation [Eq. (1)]:

$$i = -n_e F A D_{app}^{1/2} C/(\pi t)^{1/2} \quad (1)$$

in which n_e, F, A, and C refer to the number of electrons, the Faraday constant, the electrode area, and the concentration of redox sites in the film, respectively, and the i–$t^{-1/2}$ plot is linear until the diffusion layer reaches the film surface on the solution side.[20]

Figure 6 displays the current–time plots after the potential step from 0.96 to 0.36 V versus Fc^+/Fc (Fc = ferrocenyl) to reduce the Fe^{II}-complex moieties in the linear Fe(tpy)$_2$-oligomer wires [2 Fe**3**], [4 Fe**3**], [6 Fe**3**], and [8 Fe**3**] in Bu_4NClO_4/CH_2Cl_2 (0.1 and 1 mol dm^{-3}, respectively; see the Supporting Information for the PSCA results in solutions of other electrolyte concentrations). In all cases, the curvatures for the Fe^{III}/Fe^{II} couple show a quasiplateau region in the initial period, followed by a rapid decrease in current. These features are entirely different from those of the typical current-decay curves in the diffusion-limited case of the previous redox polymers,[20] because no straight-line region intersects with the origin in the i versus $t^{-1/2}$ plot (see the Supporting Information).

There are two possible rationales that can be used to interpret the i–t characteristics in the present study. One is the contribution of the ohmic resistance of the film. The time dependency does not appear if the resistance is constant, but uncommon i–t behavior may be observed when the resistance changes with time. For example, Stojek and coworkers reported uncommon i–t characteristics of redox species in a solution without an electrolyte salt in PSCA, in which the resistance is initially so high that it slows electron transport, but the gradual formation of an "excess-electrolyte zone" decreases the resistance.[21] This tendency towards an increase in current is balanced against the decreasing current due to thickening of the diffusion layer to afford complex current–time characteristics in PSCA, and the shape of the i–t curve changes drastically as the electrolyte concentration increases. This behavior is not consistent with the results shown in Figure 6, in which a quasiplateau region appears in all i–t curves, even at high electrolyte concentrations (2 mol dm^{-3}).

The other possible rationale for the uncommon i–t characteristics is an intrawire rather than a diffusional electron-transport pathway. This mechanism would explain not only

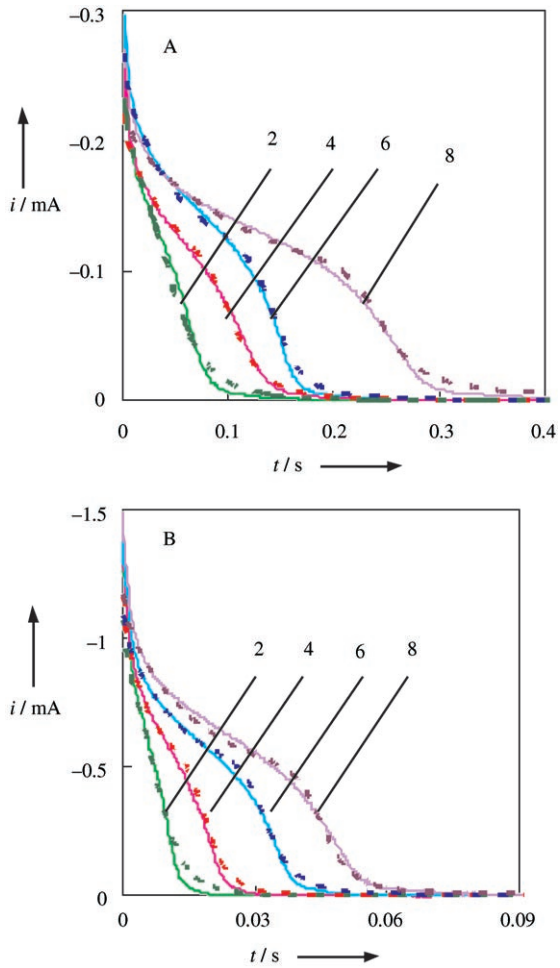

Figure 6. Current–time plots after the potential step from 0.96 to 0.36 V versus Fc^+/Fc to reduce the Fe^{III}-complex moieties in [*n* Fe**3**] ($n = 2$, 4, 6, and 8) with $t_1 = 5$ min in Bu_4NClO_4/CH_2Cl_2 (0.1 mol dm^{-3} (A) and 1 mol dm^{-3} (B); solid lines). The numbers assigned to the curves refer to *n*. Simulated curves (dotted lines) were obtained with A) $k_1 = 46$ s^{-1}, $k_2(\mathbf{3}) = 2.4 \times 10^{12}$ cm^2 mol^{-1} s^{-1}, and $C_{dl} = 18$ μC cm^{-2} for [2 Fe**3**]; $k_1 = 46$ s^{-1}, $k_2(\mathbf{3}) = 2.4 \times 10^{12}$ cm^2 mol^{-1} s^{-1}, and $C_{dl} = 20$ μC cm^{-2} for [4 Fe**3**]; $k_1 = 52$ s^{-1}, $k_2(\mathbf{3}) = 2.4 \times 10^{12}$ cm^2 mol^{-1} s^{-1}, and $C_{dl} = 29$ μC cm^{-2} for [6 Fe**3**]; $k_1 = 40$ s^{-1}, $k_2(\mathbf{3}) = 2.0 \times 10^{12}$ cm^2 mol^{-1} s^{-1}, and $C_{dl} = 60$ μC cm^{-2} for [8 Fe**3**]; B) $k_1 = 240$ s^{-1}, $k_2(\mathbf{3}) = 1.7 \times 10^{13}$ cm^2 mol^{-1} s^{-1}, and $C_{dl} = 10$ μC cm^{-2} for [2 Fe**3**]; $k_1 = 240$ s^{-1}, $k_2(\mathbf{3}) = 1.7 \times 10^{13}$ cm^2 mol^{-1} s^{-1}, and $C_{dl} = 12$ μC cm^{-2} for [4 Fe**3**]; $k_1 = 210$ s^{-1}, $k_2(\mathbf{3}) = 1.6 \times 10^{13}$ cm^2 mol^{-1} s^{-1}, and $C_{dl} = 27$ μC cm^{-2} for [6 Fe**3**]; $k_1 = 210$ s^{-1}, $k_2(\mathbf{3}) = 1.2 \times 10^{13}$ cm^2 mol^{-1} s^{-1}, and $C_{dl} = 40$ μC cm^{-2} for [8 Fe**3**].

the *i*–*t* characteristics for both linear and branched polymer wires, but also the change in the kinetics with the electrolyte concentration, as shown below.

Analysis of the *i*–*t* behavior was attempted by employing the electron-transfer mechanism in a single molecular wire on the basis of a sequential chemical reaction on a molecular level (Figure 7). When the oxidized form in the film of

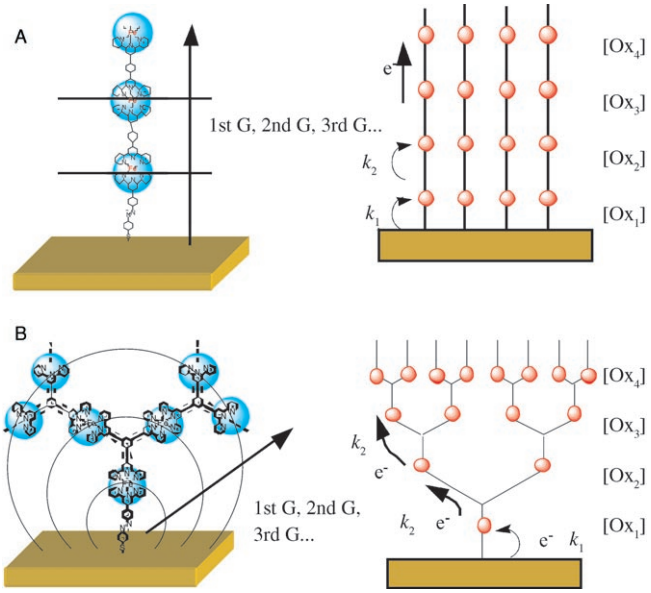

Figure 7. Schematic illustration of the electron-transfer mechanism in A) linear and B) branched molecular wires. G = generation.

molecular wires, Ox, is reduced to Red, and the back electron transfer can be neglected by applying a sufficient overpotential in PSCA, electron-transfer kinetics in the case of the *n*th complex in the sequence can be written as follows [Eq. (2)]:

$$Ox_1 + e^- \rightarrow Red_1 \text{ rate constant : } k_1 \quad (2a)$$

$$Red_1 + Ox_2 \rightarrow Ox_1 + Red_2 \text{ rate constant : } k_2 \quad (2b)$$

$$Red_2 + Ox_3 \rightarrow Ox_2 + Red_3 \text{ rate constant : } k_2 \quad (2c)$$

$$Red_{n-1} + Ox_n \rightarrow Ox_{n-1} + Red_n \text{ rate constant : } k_2 \quad (2d)$$

in which Red_i and Ox_i are the reduced and oxidized forms, respectively, in the *i*th layer or generation in the film, and, in [Eq. (3)]:

$$d[Ox_1]/dt = -k_1[Ox_1] + k_2([Ox_1]_0 - [Ox_1])[Ox_2] \quad (3a)$$

$$d[Ox_2]/dt = -k_2([Ox_1]_0 - [Ox_1])[Ox_2] + ([Ox_3]_0/[Ox_2]_0)k_2([Ox_2]_0 - [Ox_2])[Ox_3] \quad (3b)$$

$$d[Ox_3]/dt = -([Ox_3]_0/[Ox_2]_0)k_2([Ox_2]_0 - [Ox_2])[Ox_3] + ([Ox_4]_0/[Ox_2]_0)k_2([Ox_3]_0 - [Ox_3])[Ox_4] \quad (3c)$$

$$d[Ox_{n-1}]/dt = -([Ox_{n-1}]_0/[Ox_{n-2}]_0)k_2([O_{n-2}]_0 - [Ox_{n-2}])[Ox_{n-1}] + ([Ox_n]_0/[Ox_{n-2}]_0)k_2([Ox_{n-1}]_0 - [Ox_{n-1}])[Ox_n] \quad (3d)$$

$$d[Ox_n]/dt = -([Ox_n]_0/[Ox_{n-2}]_0)k_2([Ox_{n-1}]_0 - [Ox_{n-1}])[Ox_n] \quad (3e)$$

in which $[Ox_i]_0$ and $[Ox_i]$ are the initial and present two-dimensional concentrations, respectively, of the oxidized form of the redox moiety in the *i*th layer or generation, in mol cm^{-2}. The reaction kinetics are controlled by two factors: k_1 (s^{-1}), for the electron transfer between the nearest redox site and the electrode (the electron-transfer model for four complex layers is described), and k_2 (cm^2 mol^{-1} s^{-1}), for the electron transfer between neighboring redox sites in a molecular wire (in a primary approximation, the rate constant for electron transfer between neighboring sites in a polymer wire is constant). In the case of [*n*Fe**3**] [Eq. (4)],

$$[Red_1] + [Ox_1] = [Red_2] + [Ox_2] = [Red_3] + [Ox_3] = \ldots = [Red_n] + [Ox_n] = \text{constant} \quad (4)$$

The actual current can be observed as $d[Ox_1]/dt$. If the electron transfer between neighboring redox sites is faster than that between the nearest redox site and the electrode, the reaction kinetics can be regarded as "zero order", which implies that a constant current flows in the initial period. A simulation was carried out in a numerical calculation, in which the double-layer capacitance (C_{dl}), which decays exponentially with time, was taken into consideration. In the case of [*n*Fe**3**] ($n = 2$, 4, 6, and 8) in Bu_4NClO_4/CH_2Cl_2 (1 mol dm^{-3}), the curves simulated by using the single-wire redox-conduction kinetics with the parameters $k_1 = (220 \pm 10)$ s^{-1}, k_2(**3**) $= (1.4 \pm 0.1) \times 10^{13}$ cm^2 mol^{-1} s^{-1}, and $C_{dl} = (25 \pm 15)$ μC cm^{-2} reproduced all experimental results quite well, as shown in Figure 6B. (The results in an electrolyte solution of concentration 0.1 mol dm^{-3} were also reproduced with a set of k_1 and k_2 values, as shown in Figure 6A).

We simulated the results for the films of branched oligomer wires [*n*Fe**4**] by assuming a similar electron-transport mechanism with k_1 and k_2 as kinetic parameters; in this case the flux of electrons diverges along the molecular wire [Eq. (5)]:

$$[Ox_1] + [Red_1] = ([Ox_2] + [Red_2])/3 = ([Ox_3] + [Red_3])/7 = \ldots = [Red_n] + [Ox_n]/(2^n - 1) = \text{constant} \quad (5)$$

The PSCA measurements for this branched oligomer wire in Bu_4NClO_4/CH_2Cl_2 (0.1 and 1 mol dm^{-3}, respectively) showed constant-current-flow behavior over a much longer time period (≈0.6 and 0.1 s, respectively, for [4Fe**4**]; Figure 8) than for the linear wires described above (≈0.3 and 0.05 s, respectively, for [8Fe**3**]; Figure 6; see the Supporting Information for the PSCA results in solutions of other electrolyte concentrations). This difference strongly

CHEMISTRY
AN ASIAN JOURNAL

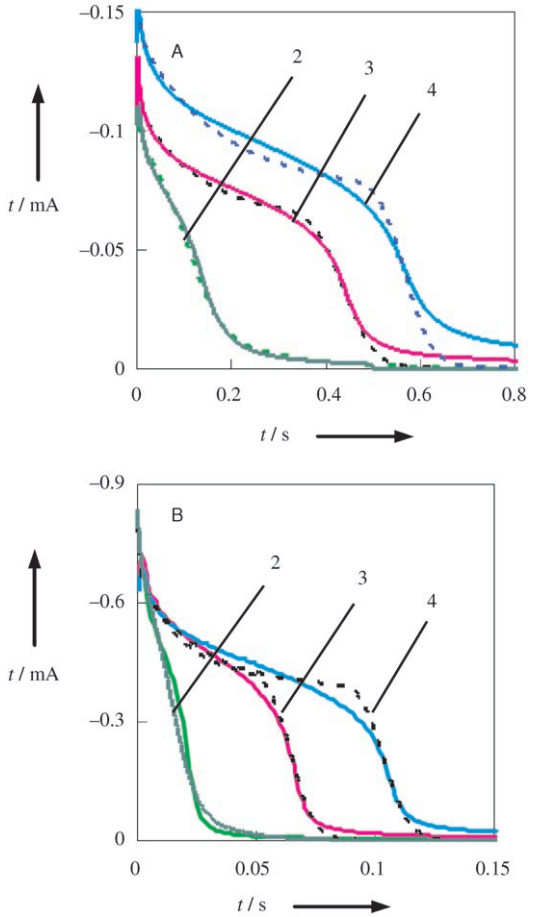

Figure 8. Current–time plots after the potential step from 0.96 to 0.36 V versus Fc^{+}/Fc to reduce the Fe^{II}-complex moieties in [*n*Fe**4**] (*n* = 2, 3, and 4) with t_1 = 5 min in Bu_4NClO_4/CH_2Cl_2 (0.1 mol dm^{-3} (A) and 1 mol dm^{-3} (B); solid lines). The numbers assigned to the curves refer to *n*. Simulated curves (dotted lines) were obtained with A) $k_1 = 38\ s^{-1}$, $k_2(\mathbf{4}) = 7.7\times10^{11}$ cm^2 mol^{-1} s^{-1}, and $C_{dl} = 23\ \mu C\,cm^{-2}$ for [2Fe**4**]; $k_1 = 40\ s^{-1}$, $k_2(\mathbf{4}) = 7.9\times10^{11}$ cm^2 mol^{-1} s^{-1}, and $C_{dl} = 23\ \mu C\,cm^{-2}$ for [3Fe**4**]; $k_1 = 49\ s^{-1}$, $k_2(\mathbf{4}) = 8.5\times10^{11}$ cm^2 mol^{-1} s^{-1}, and $C_{dl} = 42\ \mu C\,cm^{-2}$ for [4Fe**4**]; B) $k_1 = 270\ s^{-1}$, $k_2(\mathbf{4}) = 4.9\times10^{12}$ cm^2 mol^{-1} s^{-1}, and $C_{dl} = 19\ \mu C\,cm^{-2}$ for [2Fe**4**]; $k_1 = 270\ s^{-1}$, $k_2(\mathbf{4}) = 5.0\times10^{12}$ cm^2 mol^{-1} s^{-1}, and $C_{dl} = 19\ \mu C\,cm^{-2}$ for [3Fe**4**]; $k_1 = 260\ s^{-1}$, $k_2(\mathbf{4}) = 4.4\times10^{12}$ cm^2 mol^{-1} s^{-1}, and $C_{dl} = 27\ \mu C\,cm^{-2}$ for [4Fe**4**].

indicates the dominance of the through-bond electron-transport pathway, because the density of redox sites in the branched-oligomer film is expected to be similar to or higher than that in the linear-oligomer films. Thus, a simple diffusion process involving through-space electron transfer would give similar or faster kinetics of electron transport in the former than in the latter. In contrast, the observation of slower kinetics of electron transport in the branched oligomer wires is reasonable if through-bond electron transport is dominant, as the ratio of the number of molecular wires directly attached to the electrode surface to the number of redox sites in the film is smaller for the branched oligomer wires than for the linear oligomer wires (Figure 7). We simulated the *i*–*t* curves for the film of [*n*Fe**4**] (*n* = 2, 3, and 4) in Bu_4NClO_4/CH_2Cl_2 (1 mol dm^{-3}) by considering only that the through-bond electron transfer occurs between redox sites with parameters $k_1 = (260\pm10)\ s^{-1}$ and $k_2(\mathbf{4}) = (4.8\pm0.2)\times10^{12}$ cm^2 mol^{-1} s^{-1}, and with the inclusion of a C_{dl} value of $(23\pm4)\ \mu C\,cm^{-2}$. The similarity of the k_1 values for [*n*Fe**3**] and [*n*Fe**4**] is logical, because the first Fe layer is the same in both cases. The smaller $k_2(\mathbf{4})$ value for the branched oligomer wire than that for the linear wire ($k_2(\mathbf{3}) = (1.4\pm0.1)\times10^{13}$ cm^2 mol^{-1} s^{-1}) is appropriate because the bridging ligand is *m*-phenylene in the former and *p*-phenylene in the latter; thus, the branched oligomer wire has shorter π conjugation.

Figure 9 shows the dependence of the k_1 and k_2 values for [*n*Fe**3**] and [*n*Fe**4**] on the electrolyte concentration. All *i*–*t*

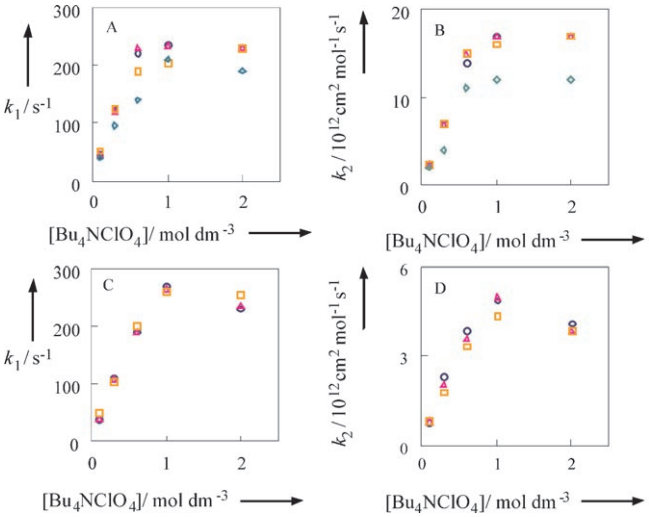

Figure 9. Dependence of the A) k_1 and B) k_2 values for [*n*Fe**3**] (t_1 = 5 min), and of the C) k_1 and D) k_2 values for [*n*Fe**4**] (t_1 = 5 min) on the electrolyte concentration in Bu_4NClO_4/CH_2Cl_2; *n* = 2 (○), 4 (△), 6 (□), and 8 (◇).

characteristics at a given electrolyte concentration could be simulated for different wire generations *n* by using similar k_1 and k_2 values, which supports the validity of this approach. The strong dependence of k_1 and k_2 on the electrolyte concentration is reasonable, because it is known that electron hopping is limited by the motion of the counterion.[12]

The electric field is an important factor in the control of the electrode kinetics. The dependence of the k_1 and k_2 values on the applied potential in PSCA measurements of [*n*Fe**3**] and [*n*Fe**4**] is shown in Figure 10. Both the k_1 and k_2 values increased exponentially with the applied potential, as expected for electrode reaction kinetics.[22] The intersection of the linear lines in the cathodic and anodic regions of the plots of $\log k_1$ or $\log k_2$ versus potential gives the intrinsic kinetic parameters k_1^0 and k_2^0 without overpotential effects. The values obtained were $k_1^0 = 110\ s^{-1}$, $k_2^0 = 2.6\times10^{12}$ cm^2 mol^{-1} s^{-1} for [*n*Fe**3**], and $k_1^0 = 100\ s^{-1}$, $k_2^0 = 4.1\times10^{11}$ cm^2 mol^{-1} s^{-1} for [*n*Fe**4**].

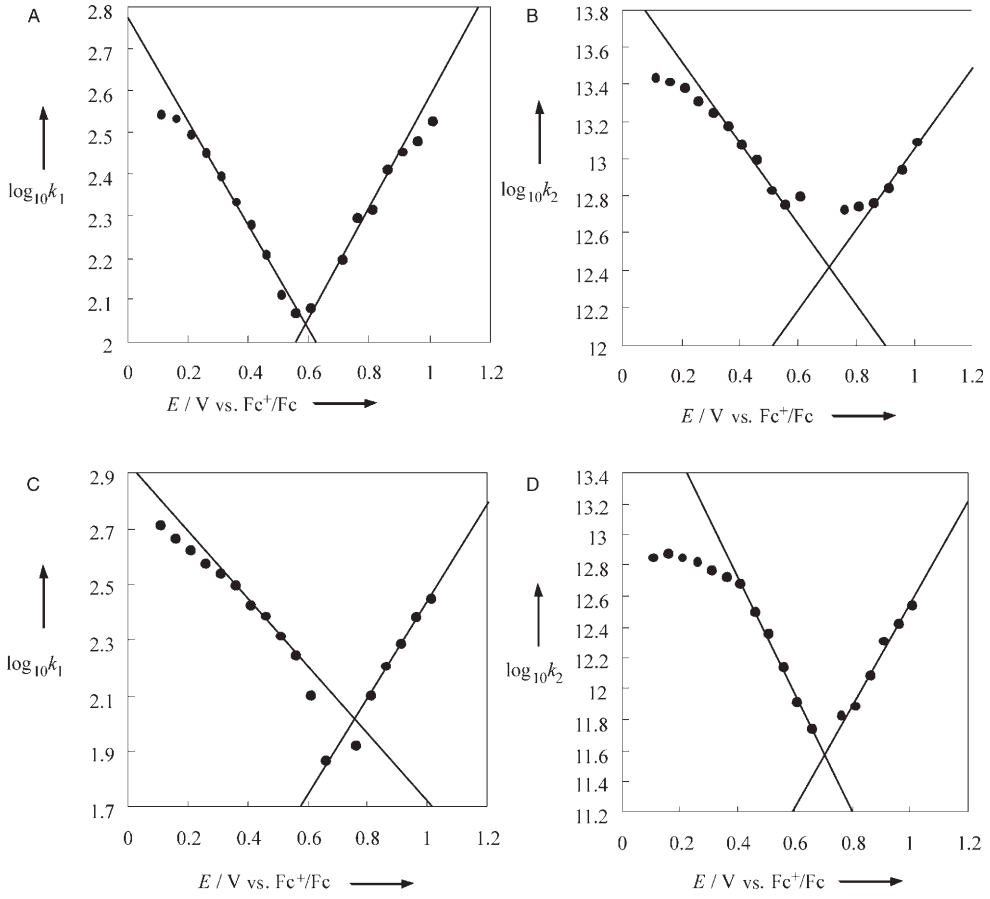

Figure 10. Dependence of A) $\log k_1$ and B) $\log k_2$ for [*n*Fe**3**] ($t_1 = 5$ min), and of C) $\log k_1$ and D) $\log k_2$ for [*n*Fe**4**] ($t_1 = 5$ min) on the potential in Bu_4NClO_4/CH_2Cl_2 (1 mol dm^{-3}).

Conclusions

In this study, we fabricated redox films with highly organized structures of molecular wires on a gold surface by using stepwise coordination reactions of metal ions and bridging ligands. This method can be used to prepare metal-complex oligomer (and polymer) wires with a desired connection network made up of a desired number of redox units. A two-way bridging ligand, **3**, gave linear oligomer wires, and a three-way bridging ligand, **4**, gave branched oligomer wires of $Fe(tpy)_2$ units. Owing to the highly organized structures, we observed unique *i–t* characteristics by PSCA. Such structures have not been reported previously for redox polymers with a low ordering of molecular wires. These *i–t* characteristics of both linear and branched redox-oligomer wires could be interpreted by a mechanism for through-bond electron transport by using two kinetic factors: k_1 (s^{-1}), for the electron transfer between the nearest redox site and the electrode (the electron-transfer model for four complex layers was described), and k_2 ($cm^2 mol^{-1} s^{-1}$), for the electron transfer between neighboring redox sites in a molecular wire. This new type of redox-polymer film will be useful for the study and development of molecular electronics.

Experimental Section

General

Tetra-*n*-butylammonium perchlorate (obtained from Tokyo Chemical Industry) was recrystallized from HPLC-grade ethanol and dried under vacuum for 24 h. Diethyl ether (Showa), hexane, and methanol (Godo) were purchased from commercial sources. Other reagents and solvents were purchased from Kanto Chemical and used as received. Water was purified by passage through a Milli-Q purification system (Millipore). Ligands **1**[23] and **2**[16a] were prepared according to the methods described in the literature. Ligand **3** and phenyl disulfide were purchased from Aldrich and used as received. ^{1}H NMR spectra were recorded with a JNM-AL400 spectrometer (JEOL). MALDI-TOF MS spectra were recorded with a Shimadzu Kratos AXIMA-CFR spectrometer.

Syntheses

4: Solid [$Pd(PPh_3)_4$] (0.19 g, 0.17 mmol) was added to a solution of tpy–C≡C*S*nBu_3 (2.2 g, 4.0 mmol)[24] in *N*,*N*-dimethylformamide (DMF; 200 mL), and the resulting mixture was heated to 100 °C. A solution of 1,3,5-tribromobenzene (0.32 g, 1.0 mmol) in DMF (50 mL) was added, and the mixture was stirred for 40 min at 100 °C, then cooled to room temperature. Compound **4** (0.55 g, 65 %) was isolated as a white powder by filtration and washed with hexane and diethyl ether. ^{1}H NMR (400 MHz, $CDCl_3$): $\delta = 7.37$ (ddd, $J = 7.8$, 4.8, 1.5 Hz, 6H), 7.79 (s, 3H), 7.89 (td, $J = 7.8$, 1.5 Hz, 6H), 8.64 (s, 6H), 8.64 (d, $J = 7.8$ Hz, 6H), 8.75 ppm (d, $J = 4.8$ Hz, 6H); MS (MALDI-TOF): *m*/*z* calcd for $C_{57}H_{34}N_9$: 844.29 $[M+H]^+$; found: 844.07; elemental analysis: calcd (%) for $C_{57}H_{33}N_9$: C 81.12, H 3.94, N 14.94; found: C 0.91, H 4.18, N 14.72.

Film Preparation

Au/mica plates (gold (100 nm) was deposited on natural mica) were used for the electrochemical measurements and annealed with a hydrogen flame just before use. This treatment gave an Au(111)-like surface consisting of Au single-crystal grains of 400–600 nm in diameter. For the preparation of [*n*Fe**3**] and [*n*Fe**4**], an Au–S–C_6H_4N=NC_6H_4–tpy SAM was prepared by immersion of an Au/mica plate in a solution of **1** (0.1 mmol dm^{-3}) in chloroform for 5 min, followed by rinsing of the plate with HPLC-grade chloroform and drying by blowing with nitrogen. To attach Fe^{II} ions, the tpy-terminated surface was immersed in aqueous $Fe(BF_4)_2$ (0.1 mol dm^{-3}) for 3 h, then washed with water and ethanol, and dried by blowing with nitrogen. To make bis(tpy)iron complexes, the metal-terminated surface was immersed in a solution of **3** or **4** (0.1 mmol dm^{-3}) in chloroform for 3 h, then washed with chloroform and dried. These last two processes (immersion in a solution of Fe^{II} ions, then in a solution of the ligand) were repeated for the preparation of films of oligomers with two iron(II) centers, each coordinated to two tpy ligands. The film of [1Fe**3**–(*n*−1)Fe**4**] was prepared by immersion of an Au/mica plate in a solution of phenyl disulfide (1 mmol dm^{-3}) in chloroform for 5 h, followed by rinsing with chloroform and drying by blowing with nitrogen. Next, to cover the surface sparsely with tpy-terminated molecules, the plate was immersed in a solution of **1** (0.1 mmol dm^{-3}) for 10 s. The plate was then immersed in aqueous $Fe(BF_4)_2$ (0.1 mol dm^{-3}) for 3 h, washed with water and ethanol, and dried. Next, the plate was immersed in a solution of **3** for 3 h, washed with chloroform, and dried. The plate was then immersed alternately in an aqueous solution of $Fe(BF_4)_2$ (0.1 mol dm^{-3}) and a solution of **4** (0.1 mmol dm^{-3}) in chloroform, with the corresponding washing and drying processes.

Electrochemical Measurements

Electrochemical measurements were carried out by using an Au/mica working electrode (electrode area: 0.264 cm^2) covered by a metal-complex film, a Pt-wire counterelectrode, and an Ag/Ag^+ reference electrode ($AgNO_3$ (10 mmol dm^{-3}) in Bu_4NClO_4/MeCN (0.1 mol dm^{-3})) in a standard one-compartment cell. Cyclic voltammetry and chronoamperometry were performed by using an ALS 750 A electrochemical analyzer. All experiments were carried out under argon at 25 °C.

STM Measurements

STM measurements were made with a Pico SPM analyzer (Molecular Imaging). The tips (Pt/Ir = 4:1, ϕ = 0.25 mm) were cut sharply and set on an A-STM scanner. The tunneling current and the bias voltage were 0.3 nA and 1.0 V, respectively.

Acknowledgements

This research was supported by Grants-in-Aid for Scientific Research (Nos. 16074204 (area 434) and 17205007), a grant from The 21st Century COE Program for Frontiers in Fundamental Chemistry of MEXT, and CREST, JST, Japan.

[1] H. B. Gray, J. R. Winkler, *Proc. Natl. Acad. Sci. USA* **2005**, *102*, 3534–3539.

[2] a) C. Joachim, J. K. Gimzewski, A. Aviram, *Nature* **2000**, *408*, 541–548; b) J. Park, A. N. Pasupathy, J. I. Goldsmith, C. Chang, Y. Yaish, J. R. Petta, M. Rinkoski, J. P. Sethna, H. D. Abruña, P. L. McEuen, D. C. Ralph, *Nature* **2002**, *417*, 722–725; c) C. E. D. Chidsey, R. W. Murray, *Science* **1986**, *231*, 25–31; d) M. S. Wrighton, *Science* **1986**, *231*, 32–37.

[3] a) C. E. D. Chidsey, *Science* **1991**, *251*, 919–922; b) H. O. Finklea, D. D. Hanshew, *J. Am. Chem. Soc.* **1992**, *114*, 3173–3181; c) M. T. Carter, G. K. Rowe, J. N. Richardson, L. M. Tender, R. H. Terrill, R. W. Murray, *J. Am. Chem. Soc.* **1995**, *117*, 2896–2899; d) K. Weber, L. Hockett, S. Creager, *J. Phys. Chem. B* **1997**, *101*, 8286–8291.

[4] a) G. K. Ramachandran, T. J. Hopson, A. M. Rawlett, L. A. Nagahara, A. Primak, S. M. Linsay, *Science* **2003**, *300*, 1413–1416; b) L. A. Bumm, J. J. Arnold, M. T. Cygan, T. D. Dunbar, T. P. Burgin, L. Jones II, D. L. Allara, J. M. Tour, P. S. Weiss, *Science* **1996**, *271*, 1705–1707; c) S. B. Sachs, S. P. Dudek, R. P. Hsung, L. R. Sita, J. F. Smalley, M. D. Newton, S. W. Feldberg, C. E. D. Chidsey, *J. Am. Chem. Soc.* **1997**, *119*, 10563–10564; d) A.-A. Dhirani, R. W. Zehner, R. P. Hsung, P. Guyot-Sionnest, L. R. Sita, *J. Am. Chem. Soc.* **1996**, *118*, 3319–3320.

[5] a) D. B. Hall, R. E. Holmlin, J. K. Barton, *Nature* **1996**, *382*, 731–735; b) M. D. Purugganan, C. V. Kumar, N. J. Turro, J. K. Barton, *Science* **1988**, *241*, 1645–1649; c) C. J. Murphy, M. R. Arkin, Y. Jenkins, N. D. Ghatlia, S. H. Bossmann, N. J. Turro, J. K. Barton, *Science* **1993**, *262*, 1025–1029; d) P. Fromherz, B. Rieger, *J. Am. Chem. Soc.* **1986**, *108*, 5361–5362; e) A. M. Brun, A. Harriman, *J. Am. Chem. Soc.* **1992**, *114*, 3656–3660.

[6] a) H.-B. Kraatz, *Macromol. Symp.* **2003**, *196*, 39–44; b) M. M. Galka, H.-B. Kraatz, *ChemPhysChem* **2002**, *3*, 356.

[7] a) P. G. Pickup, R. W. Murray, *J. Am. Chem. Soc.* **1983**, *105*, 4510–4514; b) P. G. Pickup, W. Kutner, C. R. Leidner, R. W. Murray, *J. Am. Chem. Soc.* **1984**, *106*, 1991–1998; c) E. D. Chidsey, R. W. Murray, *J. Phys. Chem.* **1986**, *90*, 1479–1484; d) J. Hjelm, R. W. Handel, A. Hagfeldt, E. C. Constable, C. E. Housecroft, R. J. Forster, *Inorg. Chem.* **2005**, *44*, 1073–1081; e) G. Zotti, G. Schiavon, S. Zecchin, A. Berlin, G. Pagani, A. Canavesi, *Synth. Met.* **1996**, *76*, 255–258.

[8] a) R. W. Murray, *Annu. Rev. Mater. Sci.* **1984**, *14*, 145–169; b) H. Nishihara, K. Aramaki, *J. Chem. Soc. Chem. Commun.* **1985**, 709–710; c) H. Nishihara, K. Aramaki, *Chem. Lett.* **1986**, 1063–1064; d) H. Nishihara, M. Noguchi, K. Aramaki, *Inorg. Chem.* **1987**, *26*, 2862–2869; e) K. Sakamoto, H. Nishihara, K. Aramaki, *J. Chem. Soc. Dalton Trans.* **1992**, 1877–1882.

[9] a) P. G. Pickup, R. W. Murray, *J. Electrochem. Soc.* **1984**, *131*, 833–839; b) H. C. Hurrell, H. D. Abruña, *Inorg. Chem.* **1990**, *29*, 736–741; c) J. Ochmanska, P. G. Pickup, *J. Electroanal. Chem. Interfacial. Electrochem.* **1991**, *297*, 197–210; d) S. S. Zhu, T. M. Swager, *J. Am. Chem. Soc.* **1997**, *119*, 12568–12577.

[10] a) H. J. Dahms, *J. Phys. Chem.* **1968**, *72*, 362–364; b) I. Ruff, V. J. Friedrich, *J. Phys. Chem.* **1972**, *76*, 162–168.

[11] D. N. Blauch, J.-M. Savéant, *J. Am. Chem. Soc.* **1992**, *114*, 3323–3332.

[12] a) R. P. Buck, *J. Phys. Chem.* **1988**, *92*, 4196–4200; b) J.-M. Savéant, *J. Electroanal. Chem. Interfacial. Electrochem.* **1987**, *242*, 1–8; c) J.-M. Savéant, *J. Electroanal. Chem. Interfacial. Electrochem.* **1988**, *242*, 1–21; d) J.-M. Savéant, *J. Phys. Chem.* **1988**, *92*, 1011–1013; e) J.-M. Savéant, *J. Phys. Chem.* **1988**, *92*, 4526–4532.

[13] A. J. Bard, L. R. Faulkner, *Electrochemical Methods: Fundamentals and Applications*, *2nd ed.*, Wiley, New York, **2001**.

[14] a) M. Abe, T. Michi, A. Sato, T. Kondo, W. Zhou, S. Ye, K. Uosaki, Y. Sasaki, *Angew. Chem.* **2003**, *115*, 3018–3021; *Angew. Chem. Int. Ed.* **2003**, *42*, 2912–2915; b) M. Maskus, H. D. Abruña, *Langmuir* **1996**, ***12***, 4455–4462; c) M. Haga, T. Takasugi, A. Tomie, M. Ishizuya, Y. Yamada, M. D. Hossain, M. Inoue, *Dalton Trans.* **2003**, 2069–2079.

[15] K. Kanaizuka, M. Murata, Y. Nishimori, I. Mori, K. Nishio, H. Masuda, H. Nishihara, *Chem. Lett.* **2005**, *34*, 534–535.

[16] a) T. Yutaka, M. Kurihara, H. Nishihara, *Mol. Cryst. Liq. Cryst. Sci. Technol. Sect. A* **2000**, *343*, 193–198; b) T. Yutaka, M. Kurihara, K. Kubo, H. Nishihara, *Inorg. Chem.* **2000**, *39*, 3438–3439; c) T. Yutaka, I. Mori, M. Kurihara, J. Mizutani, K. Kubo, S. Furusho, K. Matsumura, N. Tamai, H. Nishihara, *Inorg. Chem.* **2001**, *40*, 4986–4995; d) T. Yutaka, I. Mori, M. Kurihara, N. Tamai, H. Nishihara, *Inorg. Chem.* **2003**, *42*, 6306–6313.

[17] M. Wanunu, A. Vaskevich, A. Shanzer, I. Rubinstein, *J. Am. Chem. Soc.* **2006**, *128*, 8341–8349.

[18] As the size of Au single-crystal grains is as large as about 0.25 μm^2, the effect of grain boundaries on the electrochemical properties of molecular wires is not taken into account in the discussion.
[19] a) H. Wackerbarth, A. P. Tofteng, K. J. Jensen, I. Chorkendorff, J. Ulstrup, *Langmuir* **2006**, *22*, 6661–6667; b) T. Albrecht, A. Guckian, A. M. Kuznetsov, J. G. Vos, J. Ulstrup, *J. Am. Chem. Soc.* **2006**, *51*, 17132–17138.
[20] a) P. Daum, J. R. Lenhard, D. Rolison, R. W. Murray, *J. Am. Chem. Soc.* **1980**, *102*, 4649–4653; b) K.-N. Kuo, R. W. Murray, *J. Electroanal. Chem. Interfacial. Electrochem.* **1982**, *131*, 37–60; c) P. Burgmayer, R. W. Murray, *J. Electroanal. Chem. Interfacial. Electrochem.* **1982**, *135*, 335–342; d) S. Nakahama, R. W. Murray, *J. Electroanal. Chem. Interfacial. Electrochem.* **1983**, *158*, 303–322; e) K. Sigehara, N. Oyama, F. C. Anson, *J. Am. Chem. Soc.* **1981**, *103*, 2552–2558; f) C. R. Martin, I. Rubinstein, A. J. Bard, *J. Am. Chem. Soc.* **1982**, *104*, 4817–4824; g) H. S. White, J. Leddy, A. J. Bard, *J. Am. Chem. Soc.* **1983**, *105*, 4811–4817; h) L. Roullier, E. Waldner, E. Laviron, *J. Electroanal. Chem. Interfacial. Electrochem.* **1982**, *139*, 199–202; i) L. Roullier, E. Waldner, *J. Electroanal. Chem. Interfacial. Electrochem.* **1985**, *187*, 97–107; j) J. G. Eaves, H. S. Munro, D. Parker, *Inorg. Chem.* **1987**, *26*, 644–650; k) R. A. Saraceno, G. H. Riding, H. R. Allcock, A. G. Ewing, *J. Am. Chem. Soc.* **1988**, *110*, 7254–7255.
[21] A. Jaworski, M. Donten, Z. Stojek, *Anal. Chim. Acta* **1995**, *305*, 106–113.
[22] R. J. Forster, L. R. Faulkner, *J. Am. Chem. Soc.* **1994**, *116*, 5444–5452.
[23] Y. Ohba, K. Kanaizuka, M. Murata, H. Nishihara, *Macromol. Symp.* **2006**, *235*, 31–38.
[24] N. D. Jones, M. O. Wolf, *Organometallics* **1997**, *16*, 1352–1354.

Received: October 10, 2006
Published online: February 8, 2007

